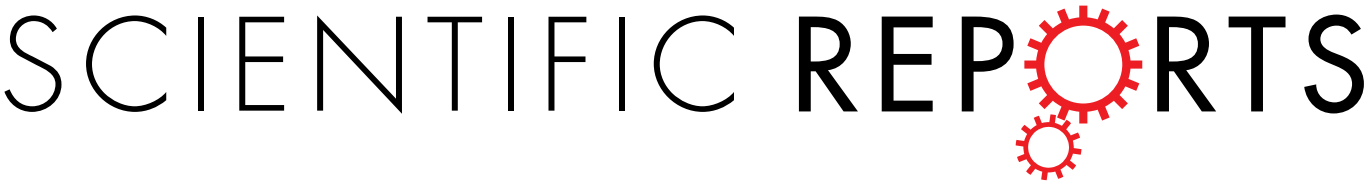

OPEN

$Be_{12}O_{12}$ Nano-cage as a Promising Catalyst for CO_2 Hydrogenation

Haiyan Zhu[1,2], Yawei Li[1,3], Guizhi Zhu[1,3], Haibin Su[1,4], Siew Hwa Chan[1,5] & Qiang Sun[1,3]

Received: 07 September 2016
Accepted: 07 December 2016
Published: 18 January 2017

An efficient conversion of CO_2 into valuable fuels and chemicals has been hotly pursued recently. Here, for the first time, we have explored a series of $M_{12}x_{12}$ nano-cages (M = B, Al, Be, Mg; X = N, P, O) for catalysis of CO_2 to HCOOH. Two steps are identified in the hydrogenation process, namely, H_2 activation to 2H*, and then 2H* transfer to CO_2 forming HCOOH, where the barriers of two H* transfer are lower than that of the H_2 activation reaction. Among the studied cages, $Be_{12}O_{12}$ is found to have the lowest barrier in the whole reaction process, showing two kinds of reaction mechanisms for 2H* (simultaneous transfer and a step-wise transfer with a quite low barrier). Moreover, the H_2 activation energy barrier can be further reduced by introducing Al, Ga, Li, and Na to $B_{12}N_{12}$ cage. This study would provide some new ideas for the design of efficient cluster catalysts for CO_2 reduction.

The energy crisis and greenhouse effect caused by the emission of carbon dioxide (CO_2) are the two serious global problems at the present day and even remain in the next 50 years[1], which stimulated the current research interest in efficient conversion of CO_2 into valuable fuels and chemicals[2–4]. However, due to the negative adiabatic electron affinity (EA) and large ionization potential (IP), the CO_2 molecule is thermodynamically stable and kinetically inert, thus making the conversion difficult under normal conditions[5]. To overcome these challenges, we need to understand the basic chemical processes of the conversion and seek for highly efficient, cost-effective, and environmentally sound catalysts. Since formic acid (FA) has been widely used as a medium for hydrogen storage and an industrial chemical, catalytic hydrogenation of CO_2 to FA becomes one of the most common and promising way to utilize CO_2.

Recently, systems containing frustrated Lewis pairs (FLPs) have been found as effective catalysts for H_2 activation[6–8], CO_2 reduction[9–11] and hydrogenation[12–14] for the production of C1 fuels. As we know that a FLP contains both Lewis acid and base centers, and the most common active Lewis pairs are B/N, B/P, Al/N and Al/P. Furthermore, a cationic Lewis acid component has also been extended to silicon[15,16], carbon[17], in ref. 9 and even the transition-metal (Zr[18,19] and Ti[20]) complexes, while the Lewis base component has been extended to O[9], carbenes[21], ethers[22], ketones[23], and sulfides[24]. The reduction of CO_2 via FLPs usually consists of two major steps: hydrogen activation and hydrogen transfer to CO_2, where a hydrogen molecule is first split into a proton (H^+) and a hydride (H^-), and then CO_2 is reduced via a concerted or sequential transfer of H^+ and H^- to CO_2. By theoretical calculations, Liu *et al.* found a relationship between these two steps, i.e. a stronger FLP results in a lower energy barrier for H_2 activation, but in a higher energy barrier for H transfer[12].

Inspired by the mechanism of CO_2 hydrogenation by FLPs, here we raise a question: whether the clusters consisting of the active element for FLPs such as B/N, B/P, Al/N and Al/P etc. could act as catalysts for H_2 splitting and CO_2 further hydrogenation?

In the past few years, experiment and theoretical research efforts have been devoted to (XY) n (M = B, Al, Be, Mg; X = N, P, O) nanostructures such as nanocages, nanohorns, nanotubes, and nanowires[25–29]. Theoretical studies found that the fullerene-like cages $(XY)_{12}$ with *Th* symmetry were the most stable geometry[30,31]. Moreover, $B_{12}N_{12}$ has been synthesized and detected by laser desorption time-of-flight mass spectrometry[32]. Al-, Ga-doped[33] and Li-, Na- decorated[34] stable $B_{12}N_{12}$ clusters have been also theoretically studied. In addition, previous studies indicated that BN[35], AlN[36,37] and BeO[38,39] clusters can absorb H_2 molecularly due to the polar bond between B and N, Al and N, Be and O with different electron affinities. Moreover BN clusters can also capture CO_2[40–42]. In fact, the most special point for cluster catalysis is that the addition or removal of a single atom can have a substantial influence on the activity and selectivity of reaction, which provides us the basis for converting

[1]Singapore-Peking University Research Centre, Campus for Research Excellence & Technological Enterprise (CREATE), 138602, Singapore. [2]Institute of Modern Physics, Northwest University, Shaanxi Key Laboratory for Theoretical Physics Frontiers, Xi'an, 710069, China. [3]Department of Materials Science and Engineering, Peking University, Beijing, 100871, China. [4]School of Materials Science and Engineering, Nanyang Technological University, 639798, Singapore. [5]School of Mechanical and Aerospace Engineering, Nanyang Technological University, 639798, Singapore. Correspondence and requests for materials should be addressed to H.Z. (email: zhuhaiyan@nwu.edu.cn)

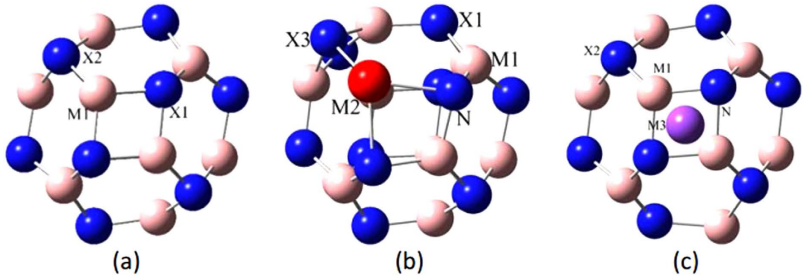

Figure 1. Geometry sketches. (**a**) MX clusters (M1 = B, Al, Be, Mg; X = N, P or O); (**b**) $AlB_{11}N_{12}$ and $GaB_{11}N_{12}$ (M2 = Al, Ga); (**c**) $LiB_{12}N_{12}$ and $NaB_{12}N_{12}$ (M3 = Li, Na).

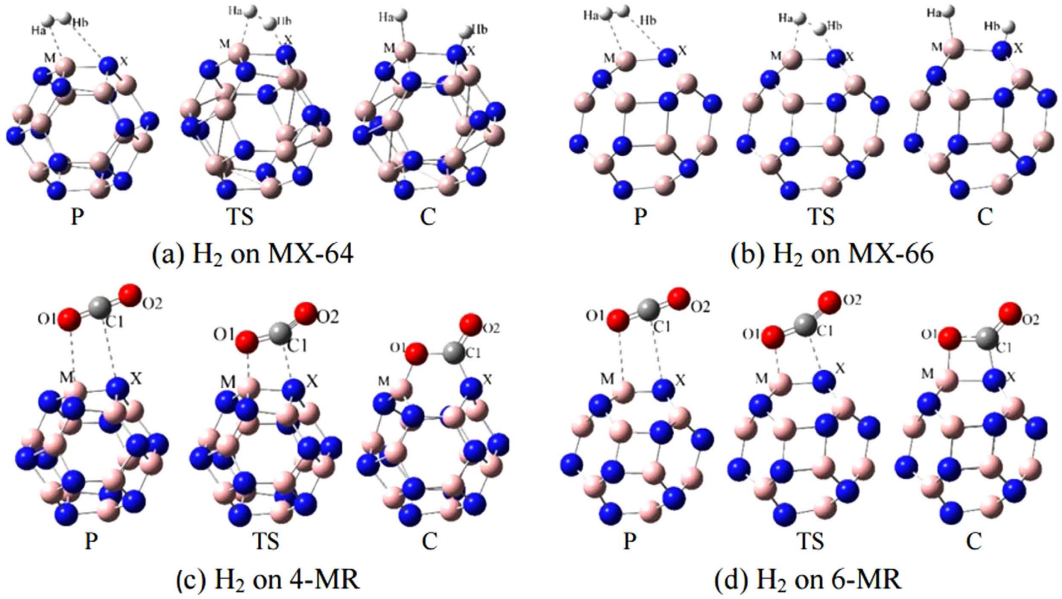

Figure 2. Geometry sketches for H2 and CO2 physiortioon (P), chemisorption (C) and the transition states (TS) in MX-64 and MX-66 configurations.

CO_2 to different products with different efficiencies by introducing different atoms to the cluster surface or inside the cluster with more flexibilities and diversities. Based on these points, in the present work we systematically study H_2 dissociation (2H*) and CO_2 hydrogenation using $M_{12}x_{12}$ (M = B, Al, Be, Mg; X = N, P, O) cage clusters, and explore the involved mechanisms.

Results and Discussions

Geometry structures. For $M_{12}x_{12}$ type cluster with T_h symmetry as $B_{12}N_{12}$, $Al_{12}N_{12}$, $B_{12}P_{12}$, $Al_{12}P_{12}$, $Be_{12}O_{12}$ and $Mg_{12}O_{12}$, they all consist of eight 6-membered rings (6-MR) and six 4-membered rings (4-MR), as was shown on Fig. 1(a). To improve the binding with CO_2 and H_2, Al, Ga [Fig. 1(b)] and Li, Na [Fig. 1(c)] are introduced to $B_{12}N_{12}$ cage, the geometry parameters can be found in Table S1 of Supporting Information, where there are two types of M-X bonds: the bond shared by two 6-MRs (labelled MX-66), and the other one shared between a 4-MR and 6-MR (labelled MX-64), the former is longer than the latter for all studied nano-cages.

H_2 and CO_2 Activation. In order to determine the configuration with the lowest energy for H_2 and CO_2 adsorption on the surface of the cluster, a number of different initial structures have been used for optimization. The results of stable $H_2/M_{12}x_{12}$, $CO_2/M_{12}x_{12}$ complexes as well as their corresponding transition state (TS) structures are shown in Fig. 2. For the convenience of discussions, we distinguish the physisorption (P) from the chemical functionalization (C) for the molecules on the cages. As seen from Fig. 2, in the process of physisorption, H_2 and CO_2 molecules are weakly adsorbed on the clusters with minor changes in geometry. While in the chemical adsorption, H_2 is dissociated forming 2H* and CO_2 is chemically activated forming CO_2*. The corresponding geometry parameters as well as their TSs are shown in Tables S2 and S3, and the interaction energies of H_2 and CO_2 physisorption and chemical absorption are given in Table S4 of Supporting Information.

The activation energies of H_2 on MX-64 and MX-66 are labeled as ΔG_1^H and ΔG_2^H, respectively, while the activation energies of CO_2 on MX-64 and MX-66 are labeled as ΔG_1^C and ΔG_2^C respectively. The energy barriers

Clusters	$B_{12}N_{12}$	$Al_{12}N_{12}$	$B_{12}P_{12}$	$Al_{12}P_{12}$	$Be_{12}O_{12}$	$Mg_{12}O_{12}$	$LiB_{12}N_{12}$	$NaB_{12}N_{12}$	$AlB_{11}N_{12}$	$GaB_{11}N_{12}$
ΔG_1^H	1.19	0.61	0.74	1.25	1.04	0.31	0.99	0.90	0.76	0.83
ΔG_2^H	1.27	0.68	1.06	1.46	1.33	0.73	1.09	0.92	0.84	0.94
ΔG_1^C	0.56	0.12	1.11	0.61	0.44	0.04	0.56	0.50	0.39	0.46
ΔG_2^C	0.51	0.11	1.06	0.63	0.47	0.03	0.33	0.26	0.36	0.43

Table 1. Gibbs energy barrier for H_2 (ΔG^H), and CO_2 activation (ΔG^C), All values are in eV.

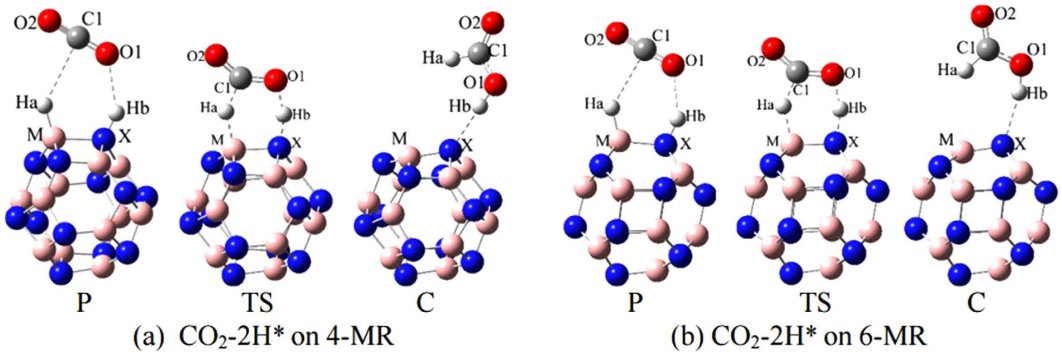

Figure 3. Geometry sketches for 2H* transfer from MX cluster to CO_2 in physisorption (P), chemisorption (C) and the transition states (TS) on MX-64 (**a**) and MX-66 (**b**) of the MX-2H* clusters.

for H_2 activation (ΔG^H) are calculated as the Gibbs energy difference between the TS^H (the TS for H_2 activation) and the initial state of H_2 adsorption:

$$\Delta G^H = G_{TS}^H - G_p^H \tag{1}$$

Similarly, the energy barriers for the CO_2 activation (ΔG^C) are calculated as the Gibbs energy difference between the TS^C (the TS for CO_2 activation) and the initial state of CO_2 adsorption:

$$\Delta G^C = G_{TS}^C - G_p^C \tag{2}$$

The calculated results are listed in Table 1, and typical structures with H_2 and CO_2 either in physisorption, or chemisorption as well as their transition states are given in the Fig. 2. All the Gibbs energy barrier for H_2 activation on MX-64 are all lower than which of the MX-66. When the activation barrier is overcome, H_2 can be dissociated generating hydridic (Ha) and protic (Hb) hydrogens.

Instead for CO_2 activation, the Gibbs energy barrier on MX-64 are all higher than that of the MX-66 except for $Al_{12}P_{12}$ and $Be_{12}O_{12}$ clusters. The activation barriers of CO_2 are lower than that of H_2 for the studied systems except for $B_{12}P_{12}$. The Al, Ga doped and Li, Na decorated $B_{12}N_{12}$ cages have lower activation energy barriers for H_2 and CO_2 than those of the pristine $B_{12}N_{12}$. This illustrates that the doping with Al and Ga as well as decoration with Li and Na can increase the activity of $B_{12}N_{12}$ cluster.

To clarify the effect of H_2 and CO_2 adsorptions on the electronic structures of nano-cages, natural bond orbital (NBO) analyses are performed and the results are listed in Table S5, from which one can see that upon the adsorption, charges on the cages are redistributed due to the geometry change and charge transfer. For example, in all the cases CO_2 received electrons from cages resulting in the activation. The charges on M sites in all clusters are decreased upon the H_2 adsorption, while increased upon the CO_2 adsorption.

The different behaviors in H_2 activation on MX-64 and MX-66 are due to the different activities between them. As seen from Table S5, more charges are on M and X sites in MX-64 than those in MX-66, which makes the former more active with a lower H_2 activation barrier as compared with the latter one.

2H* transfer mechanism. Two reaction pathways for CO_2 hydrogenation on Lewis pair moiety have been identified, one involves the physisorped CO_2 reacting with the chemisorbed 2H*, and the other one involves the physisorped H_2 reacting with CO_2*. For the latter, the reaction barrier for hydrogenation of the activated CO_2* is usually very high as found by Ye[12] (2.65 eV in UiO-66-P-BF_2 catalyst) and by us (2.84 eV for MX-64 and 2.97 eV for MX-66 of $B_{12}N_{12}$), and this pathway leads to the formation of chemisorbed HCO and OH ([HCO + OH]*) instead of HCOOH as shown in Supporting Information (Fig. S1). Consequently, in the following discussions, we only focused on the first path way for HCOOH formation.

According to the first pathway, CO_2 is firstly physiosorbed on MX-2H*(P), and then forms HCOOH (C) via the transition state (TS) (Fig. 3). For $B_{12}N_{12}$ nano cage, the reaction barrier for H_2 activation on MX-64 (1.19 eV) is lower than that on MX-66 (1.27 eV), while the 2H* transfer barrier on MX-64 (1.28 eV) is higher than that on MX-66 (1.19 eV). The IRC calculations show that the hydride and protons are transferred to CO_2 simultaneously.

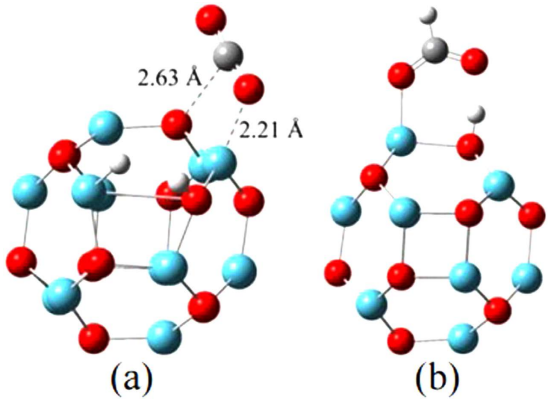

Figure 4. (**a**) Physisorption of CO_2 on $Mg_{12}O_{12}-2H^*$; (**b**) HCOOH on $Mg_{12}O_{12}-2H^*$. (The jade-blue sphere representing Mg atom, red sphere representing O atom, gray sphere representing C atom and white sphere representing H, respectively).

Clusters	$B_{12}N_{12}$	$Al_{12}N_{12}$	$B_{12}P_{12}$	$Al_{12}P_{12}$	$Be_{12}O_{12}$	$LiB_{12}N_{12}$	$NaB_{12}N_{12}$	$AlB_{11}N_{12}$	$GaB_{11}N_{12}$
ΔG_1^{HT}	1.45	1.43	2.02	1.41	0.45	2.16	1.75	2.05	2.25
ΔG_2^{HT}	1.40	1.36	1.91	1.47	0.24	1.49	1.51	1.89	2.06

Table 2. Gibbs energy barrier for H_2 transfer (ΔG^{HT}) to form HCOOH, all values are in eV.

In other words, the H transfer step is essentially the donation of a hydride and a proton from the ion-pair products to CO_2 via a concerted mechanism. Tables S6 and S7 list the corresponding geometry parameters, transition states, and interaction energies for CO_2 and HCOOH.

When attempting to bind CO_2 with $Mg_{12}O_{12}-2H^*$ in a way shown in Fig. 3(P), we cannot find any stable structures from our calculations. While CO_2 can directly bonds at Mg and O sites (as shown in Fig. 4a) with a stronger binding energy of −0.5 eV (Table S4). Similarly, when introducing HCOOH to $Mg_{12}O_{12}$ shown in Fig. 3(C), one H atom of HCOOH was taken away by the O atom in $Mg_{12}O_{12}$ nano-cage (Fig. 4b). This suggests that $Mg_{12}O_{12}$ is not competent to be the catalyst for CO_2 hydrogenation to HCOOH.

The activation energies of H_2 transfer on MX-64 and MX-66 are labeled as ΔG_1^{HT} and ΔG_2^{HT} and respectively. The energy barriers for H_2 activation (ΔG^{HT}) are calculated as the Gibbs energy difference between the TS^{HT} (the TS for H_2 transfer) and the initial state of CO_2 the physisorbed on MX-2H*:

$$\Delta G^{HT} = G_{TS}^{HT} - G_p^{HT} \tag{3}$$

The corresponding activation energies for H_2 transfer are listed in Table 2, where one can see that the activation energies of H transfer are all higher than 1.0 eV, except for $Be_{12}O_{12}$ cage. Just the opposite to the H_2 activation process in Table 1, all the Gibbs energy barriers for 2H* transfer on MX-64 are all higher than that of MX-66.

Based on the overall consideration of H_2 activation and 2 H* transfer barriers as listed in Tables 1 and 2, one can find that introducing Al, Ga, Li, and Na to $B_{12}N_{12}$ cage has definitely decreased the H_2 activation energy barrier but increased the 2H transfer energy as compared to the pristine $B_{12}N_{12}$.

In order to be more intuitive, a potential energy surfaces of the reaction pathway are shown in Fig. 5 showing a balance between H_2 activation and H transfer. Thus, the interaction between the cluster and H_2 is extremely important, the stronger catalyst with more strength to activate the hydrogen molecule would promote a faster hydrogen activation process. On the other hand, a stronger catalyst has more strength to keep the hydrogen, thus would slow down the hydrogen transfer process. This is in accordance with the general Sabatier principle[43].

To understand the trend of protonation activation barriers for the studied nanocages, we analyze the charges on C site of CO_2. In the free standing state, C carries 1.069 e. When CO_2 is adsorbed with MX-66 configuration on $B_{12}N_{12}$-2H*, $NaB_{12}N_{12}$-2H* and $LiB_{12}N_{12}$-2H*, the charges increase to 1.086, 1.084, and 1.087 e, respectively. The increased charges on C site make it more active to easily bind H with smaller barriers. The similar mechanism can also be applied to other cages.

2H* transfer one by one with stepwise mechanism. When checking the overall the activation energy barrier of H_2 activation and transfer (seen from Tables 1 and 2), one can find that many clusters such as $Al_{12}N_{12}$, $NaB_{12}N_{12}$ and $AlB_{11}N_{12}$ etc. have lower H_2 activation but higher 2 H* transfer barriers. To search for a lower barrier of H transfer, the other mechanism needs to be investigated further. We find that a new stepwise mechanism exists for CO_2 hydrogenation only on $Be_{12}O_{12}$ cage as shown in Fig. 6.

By following this reaction mechanism, the first H transfer is a rate-limiting step-with an activation energy of 0.22 eV on MX-64 bond (red line on Fig. 6) and 0.36 eV on the MX-66 bond (blue line on Fig. 6), In contrast, the 2H* transfer activation on MX-64 and MX-66 bonds is 0.45 eV and 0.24 eV, respectively. Then, we can conclude

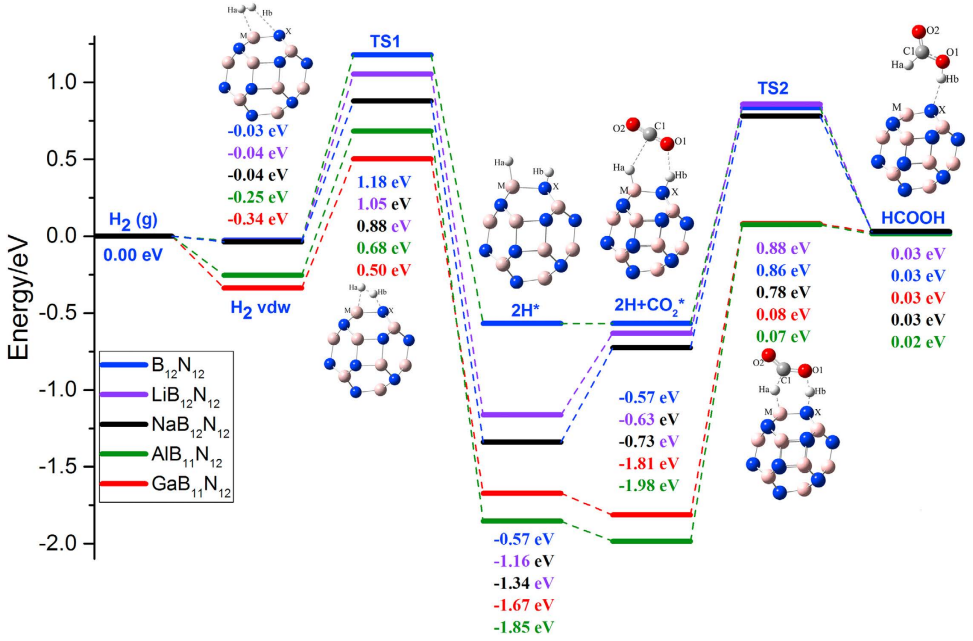

Figure 5. Relative potential energy surfaces for H_2 activation and 2H* transfer pathway in Al, Ga doped, Li, Na decorated $B_{12}N_{12}$ and pristine $B_{12}N_{12}$ with Mx-66 bond as example.

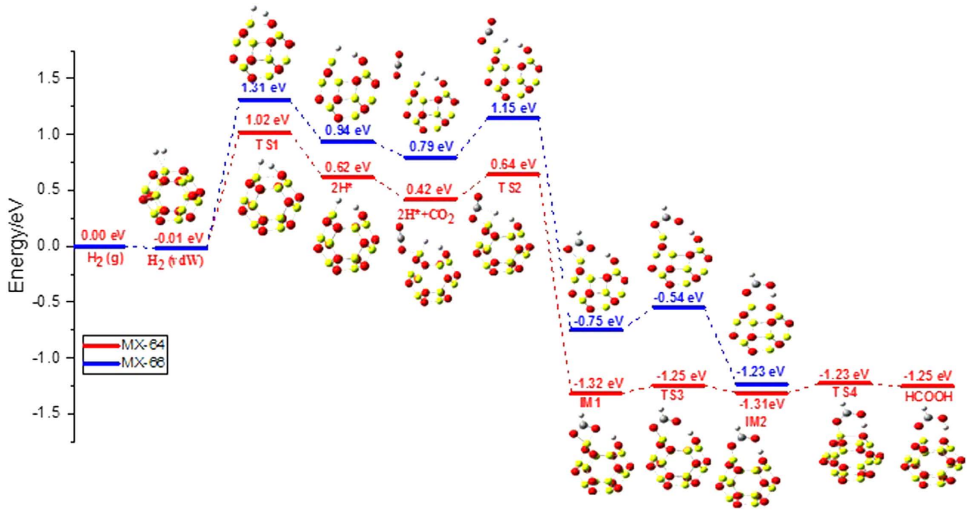

Figure 6. Relative potential energy surfaces for H_2 activation and H* stepwise transfer pathway on Mx-64 (redline) and MX-66 (blue line) bond for $Be_{12}O_{12}$. (The yellow sphere representing Be atom, red sphere representing O atom, gray sphere representing C atom and white sphere representing H, respectively).

that 2H* simultaneously transfer to CO_2 on MX-66 bond has lower activation energy than that of the one H transfer stepwise, but on MX-64 bond the situation is opposite.

For practical applications of an efficient catalyst, both the H_2 activation and transfer barriers should be comparable or lower than 1 eV[44]. Among all systems studied here, $Be_{12}O_{12}$ is the most promising catalyst, where the H_2 activation barrier is close to 1 eV (1.04 eV) on MX-64 bond, and the following H* transfer barriers are all lower than 1 eV, (0.45 eV by the 2H* simultaneously transfer mechanism, while 0.22 eV by the H* stepwise transfer mechanism). Therefore, the reaction pathway on $Be_{12}O_{12}$ MX-64 bond has the lowest barrier based on the overall consideration of the H_2 activation (1.04 eV) and H* stepwise transfer (0.22 eV).

Conclusions

In summary, based on the DFT and MP2 calculations, a series $M_{12}X_{12}$ nano-cages have been studied for activating H_2 and CO_2 to form HCOOH. The hydrogenation process mainly consists of H_2 activation to 2H*, and then 2H* further transfer to CO_2 forming a HCOOH molecule. Two kinds of H* transfer mechanisms are found: one involves 2H* simultaneous transfer, and the other is a stepwise H* transfer to CO_2. The two mechanisms result

in the same product HCOOH. Moreover, Al, Ga doped and Li, Na decorated $B_{12}N_{12}$ cages have lower H_2 activation energy barriers, but higher 2H* transfer activation barriers than that of the pristine $B_{12}N_{12}$. For practical applications, in order to have an efficient catalyst to reduce CO_2, we should search for a catalyst that has a balance between the energy barriers for H_2 activation and the H transferring. Among all the systems studied here, $Be_{12}O_{12}$ is found to be the most promising catalyst, its reaction pathway on MX-64 bond has the lowest barriers (1.04 eV for H_2 activation and 0.22 eV for H* transferring). This conclusion would motivate experimental work in the future.

Methods

Since many theoretical calculations have demonstrated that different DFT functions (e.g. B97D, ω-B97X-D, and M06-2X) and basis sets (e.g. 6–31 G*, 6–31 + G**) led to very similar results for the systems only containing main group elements for H_2 activations[7,8,11]. In this work, all the geometry optimizations are performed at the M06-2X/6–31 + G** level as implemented in Gaussian 09 package[45]. Solvent effects are taken into account by using the polarizable continuum model (PCM) with toluene as a solvent. The highly parameterized, empirical exchange correlation functional, M06-2X, developed by Zhao and Truhlar, was shown to better describe the main-group thermochemistry and kinetics than other density functionals such as B3LYP[46]. Moreover, this hybrid density M06-2X functional has been previously proved to have a good reliability in computing molecular binding energies of H_2 and CO_2 on FLPs[47]. Frequency calculations are carried out at the same level to characterize the nature of the stationary points along the reaction coordinates. No imaginary frequencies were found for the local minima, and one and only one imaginary frequency was found for the transition state. The Natural Bond Orbital (NBO 3.1) program[48], was used to calculate the natural charges at the M06-2X/6–31 + G** level of theory. The thermal contributions at room temperature (298.15 K) including the specific free energies were obtained from a harmonic analysis, and accurate electronic energies were obtained from frequency calculations using Møller-Plesset second-order perturbation theory (MP2)[49,50] with the cc-pVTZ triple-ζ quality basis[51,52]. Using the optimized geometries and starting from the TS, intrinsic reaction coordinate (IRC) calculations are performed to verify the true connection of the reactants, the transition states and the products for both H_2, CO_2 activation and H transfer processes.

References

1. Appel, A. M. *et al.* Frontiers, Opportunities, and Challenges in Biochemical and Chemical Catalysis of CO_2 Fixation. *Chem. Rev.* **113,** 6621–6658 (2013).
2. Wang, W. H., Himeda, Y., Muckerman, J. T., Manbeck, G. F. & Fujita E. CO_2 Hydrogenation to Formate and Methanol as an Alternative to Photo- and Electrochemical CO_2 Reduction. *Chem. Rev.* **115,** 12936–12973 (2015).
3. Li, Y. W., Su, H. B., Chan, S. H. & Sun, Q. CO_2 Electroreduction Performance of Transition Metal Dimers Supported on Graphene: A Theoretical Study. *ACS Catal.* **5,** 6658–6664 (2015).
4. Li, Y. W. & Sun, Q. Recent Advances in Breaking Scaling Relations for Effective Electrochemical Conversion of CO_2. *Adv. Energy Mater.* **4,** 16004631–19 (2016).
5. Li, Y. W., Chan, S. H. & Sun, Q. Heterogeneous Catalytic Conversion of CO_2: a Comprehensive Theoretical Review. *Nanoscale.* **7,** 8663–8683 (2015).
6. Sun, X. Y., Li, B., Liu, T. F., Song, J. & Su, D. S. Designing Graphene as a New Frustrated Lewis Pair Catalyst for Hydrogen Activation by Co-doping. *Phys. Chem. Chem. Phys.* **18,** 11120–11124 (2016).
7. Zeonjuk, L. L. Are Intramolecular Frustrated Lewis Pairs also Intramolecular Catalysts? A Theoretical Study on H_2 Activation. *Phys. Chem. Chem. Phys.* **17,** 10687–10698 (2015).
8. Zeonjuk, L. L. *et al.* On the Mechanism of Hydrogen Activation by Frustrated Lewis Pairs. *Chem. Eur. J.* **19(51),** 17413–17424 (2013).
9. Ghuman, K. K. *et al.* Photoexcited Surface Frustrated Lewis Pairs for Heterogeneous Photocatalytic CO_2 Reduction. *J. Am. Chem. Soc.* **138,** 1206–1214 (2016).
10. Chen, J. W., Falivene, L., Caporaso, L., Cavallo, L. & Chen, E. Y.-X. Selective Reduction of CO_2 to CH_4 by Tandem Hydrosilylation with Mixed Al/B Catalysts. *J. Am. Chem. Soc.* **138,** 5321–5333 (2016).
11. Liu, L., Vankova, N. & Heine, T. A Kinetic Study on the Reduction of CO_2 by Frustrated Lewis Pairs: from Understanding to Rational Design. *Phys. Chem. Chem. Phys.* **18,** 3567–3574 (2016).
12. Ye, J. Y. & Johnson, J. K. Design of Lewis Pair-Functionalized Metal Organic Frameworks for CO_2 Hydrogenation. *ACS Catal.* **5,** 2921–2928 (2015).
13. Courtemanche, M. A., AndréLégare, M., Maron,. L. & Fontaine, F. G. Reducing CO_2 to Methanol Using Frustrated Lewis Pairs: On the Mechanism of Phosphine–Borane-Mediated Hydroboration of CO_2. *J. Am. Chem. Soc.* **136,** 10708–10717 (2014).
14. Stephan, D. W. & Erker, G. Frustrated Lewis Pair Chemistry: Development and Perspectives. *Angew. Chem. Int. Ed.* **54,** 6400–6441 (2015).
15. Reismann, M., Schäfer, A., Jung, S. & Müller, T. Silylium Ion/Phosphane Lewis Pairs. *Organometallics* **32,** 6736–6744 (2013).
16. Herrington, T. J. *et al.* Bypassing a Highly Unstable Frustrated Lewis Pair: Dihydrogen Cleavage by a Thermally Robust Silylium–Phosphine Adduct. *Chem. Commun.* **50,** 12753–12756 (2014).
17. Clark, E. R. & Ingleson, M. J. N-Methylacridinium Salts: Carbon Lewis Acids in Frustrated Lewis Pairs for σ-bond Activation and Catalytic Reductions. *Angew. Chem. Int. Ed.* **53,** 11306–11309 (2014).
18. Xu, X., Kehr, G., Daniliu, C. G. & Erker, G. Reactions of a Cationic Geminal Zr+/P Pair with Small Molecules. *J. Am. Chem. Soc.* **135,** 6465–6476 (2013).
19. Normand, A. T. *et al.* Phosphido- and Amidozirconocene Cation-Based Frustrated Lewis Pair Chemistry. *J. Am. Chem. Soc.* **137,** 10796–10808 (2015).
20. Chapman, A. M. & Wass, D. F. Cationic Ti(IV) and Neutral Ti(III) Titanocene–Phosphinoaryloxide Frustrated Lewis Pairs: Hydrogen Activation and Catalytic Amine-Borane Dehydrogenation. *Dalton Trans.* **41,** 9067–9072 (2012).
21. Chase, P. A., Gille, A. L., Gilbert, T. M. & Stephan, D. W. Frustrated Lewis Pairs Derived from N-Heterocyclic Carbenes and Lewis Acids. *Dalton Trans.* **21,** 7179–7188 (2009).
22. Hounjet, L. J. *et al.* Combinations of Ethers and $B(C_6F_5)_3$ Function as Hydrogenation Catalysts. *Angew. Chem. Int. Ed.* **52,** 7492–7495 (2013).
23. Longobardi, L. E., Tang, C. & Stephan, D. W. Stoichiometric Reductions of Alkyl-Substituted Ketones and Aldehydes to Borinate Esters. *Dalton Trans.* **43,** 15723–15726 (2014).
24. Tanur, C. A. & Stephan, D. W. The Thioether-Methyleneborane $(PhSCH_2B(C_6F_5)_2)_2$: Synthesis and Reactivity with Donors and Alkynes. *Organometallics.* **30,** 3652–3657 (2011).

25. Li, J. L., He, T. & Yang, G. W. An all-purpose building block: $B_{12}N_{12}$ fullerene. *Nanoscale*. **4,** 1665–1670 (2012).
26. Shamlouei, H. Z., Nouri, A. Mohammadi, A. & Tehrani, A. D. Influence of transition metal atoms doping on structural, electronic and nonlinear optical properties of $Mg_{12}O_{12}$ nanoclusters: A DFT study. *Phys. E*. **77,** 48–53 (2016).
27. Shakerzdeh, E., Tahmasebi, E. & Shamlouei, H. R. The influence of alkali metals (Li, Na and K) interaction with $Be_{12}O_{12}$ and Mg12O12 nanoclusters on their structural, electronic and nonlinear optical properties: A theoretical study. *Synthetic Me*t. **204,** 17–24 (2015).
28. Beheshtian, J., Bagheri, Z., Kamfiroozi, M. & Ahmadi, A. A comparative study on the $B_{12}N_{12}$, $Al_{12}N_{12}$, $B_{12}P_{12}$ and $Al_{12}P_{12}$ fullerene-like cages. *J. Mol. Model.* **18,** 2653–2658 (2012).
29. Beheshtian, J., Kamfiroozi, M., Bagheri, Z. & Ahmadi, A. Theoretical study of hydrogen adsorption on the $B_{12}P_{12}$ fullerene-like nanocluster. *Comp. Mater. Sci*. **54,** 115–118 (2012).
30. Strout, D. L. Structure and Stability of Boron Nitrides: Isomers of $B_{12}N_{12}$. *J. Phys. Chem. A* **104,** 3364–3366 (2000).
31. Wang, R. X., Zhang, D. J. & Liu, C. B. Theoretical prediction of a novel inorganic fullerene-like family of silicon–carbon materials. *Chem. Phys. Lett.* **411,** 333–338 (2005).
32. Oku, T., Nishiwaki, A. & Narita, I. Formation and atomic structure of $B_{12}N_{12}$ nanocage clusters studied by mass spectrometry and cluster calculation. *Sci. Techol. Adv. Mat*. **5,** 635–638 (2004).
33. Shakerzadeh, E., Khodayar, E. & Noorizadeh, S. Theoretical assessment of phosgene adsorption behavior onto pristine, Al- and Ga-doped $B_{12}N_{12}$ and $B_{16}N_{16}$ nanoclusters. *Comp. Mat. Sci*. **118,** 155–171 (2016).
34. Tahmasebi, E., Shakerzadeh, E. & Biglari, Z. Theoretical assessment of the electro-optical features of the group III nitrides ($B_{12}N_{12}$, $Al_{12}N_{12}$ and $Ga_{12}N_{12}$) and group IV carbides (C_{24}, $Si_{12}C_{12}$ and $Ge_{12}C_{12}$) nanoclusters encapsulated with alkalimetals (Li, Na and K). *Appl. Surf. Sci.* **363** 197–208 (2016).
35. Sun, Q., Wang, Q. & Jena, P. Storage of Molecular Hydrogen in B−N Cage: Energetics and Thermal Stability. *Nano Lett.* **5,** 1273–1277 (2005).
36. Wang, Q., Sun, Q., Jena, P. & Kawazoe, Y. Potential of AlN Nanostructures as Hydrogen Storage Materials. *ACS Nano*. **3,** 621–626 (2009).
37. Zhou, X., Wu, M. M., Zhou, J. & Sun, Q. Hydrogen Storage in Al–N Cage Based Nanostructures. *Appl. Phys. Lett.* **94,** 103105 (2009).
38. Shinde, R. & Tayade, M. Remarkable Hydrogen Storage on Beryllium Oxide Clusters: First-Principles Calculations. *J. Phys. Chem. C.* **118,** 17200–17204 (2014).
39. Beheshtian, J. & Ravaei, I. Hydrogen Storage by BeO Nano-cage: A DFT Study. *Appl. Sur. Sci*. **368,** 76–81 (2016).
40. Guo, H. Y. *et al.* CO_2 Capture on *h*-BN Sheet with High Selectivity Controlled by External Electric Field. *J. Phys. Chem. C.* **119,** 6912–6917 (2015).
41. Sinthika, S. *et al.* Activation of CO and CO_2 on Homonuclear Boron Bonds of Fullerene-like BN Cages: First Principles Study. *Scientific Reports* **5,** 17460 (2015).
42. Sun, Q., Li, Z., Searles, D. J., Chen, Y., Lu, G. & Du, A. Charge-Controlled Switchable CO_2 Capture on Boron Nitride Nanomaterials. *J. Am. Chem. Soc.* **135,** 8246–8253 (2013).
43. Rothenberg, G. *Catalysis: Concepts and Green Applications*. (Wiley online, pp. 39–75, 2008).
44. Grabow, L. C. & Markakis, M. Mechanism of Methanol Synthesis on Cu through CO_2 and CO Hydrogenation. *ACS Catal.* **1,** 365–384 (2011).
45. Frisch, M. J. *et al.* Gaussian 09, Revision B.01, Gaussian, Inc., Wallingford, CT (2009).
46. Zhao, Y. & Truhlar, D. G. The M06 Suite of Density Functionals for Main Group Thermochemistry, Thermochemical Kinetics, Noncovalent Interactions, Excited States, and Transition Elements: Two New Functionals and Systematic Testing of Four M06-class Functionals and 12 other Functionals. *Theor. Chem. Account*. **120,** 215–241 (2008).
47. Ye, J. Y. & Johnson, J. K. Screening Lewis Pair Moieties for Catalytic Hydrogenation of CO_2 in Functionalized UiO-66. *ACS Catal*. **5,** 6219−6229 (2015).
48. Foster, J. P. & Weinhold, F. Natural Hybrid Orbitals. *J. Am. Chem. Soc*, **102,** 7211–7218 (1980).
49. Møller, C. & Plesset, M. S. Note on an Approximation Treatment for Many-Electron Systems. *Phys. Rev*. **46,** 618 (1934).
50. Pople, J. A., Binkley, J. S. & Seeger, R. Theoretical Models Incorporating Electron Correlation. *Int. J. Quantum Chem.* **10,** 1–19 (1976).
51. Dunning, T. H. Gaussian Basis Sets for Use in Correlated Molecular Calculations. I. The Atoms Boron through Neon and Hydrogen. *J. Chem. Phys.* **90,** 1007 (1989).
52. Kendall, R. A., Dunning, T. H. & Harrison, R. J. Electron Affinities of the First-row Atoms Revisited. Systematic Basis Sets and Wave Functions. *J. Chem. Phys*. **96,** 6796 (1992).

Acknowledgements

This work was partially supported by grants from the National Research Foundation (NRF) of Singapore under its Campus for Research Excellence and Technological Enterprise (CREATE) program and the National Natural Science Foundation of China (11204239) and the Double First-class University Construction project of Northwest University.

Author Contributions

H.Z. carried out the theoretical calculations and wrote the manuscript. G.Z. and Y.L. analyzed the reaction mechanism. Q.S., H.S. and S.C. designed the study.

Additional Information

Supplementary information accompanies this paper at http://www.nature.com/srep

Competing financial interests: The authors declare no competing financial interests.

How to cite this article: Zhu, H. *et al.* $Be_{12}O_{12}$ Nano-cage as a Promising Catalyst for CO_2 Hydrogenation. *Sci. Rep.* **7**, 40562; doi: 10.1038/srep40562 (2017).

Publisher's note: Springer Nature remains neutral with regard to jurisdictional claims in published maps and institutional affiliations.